PROPORTIONAL AND DRIFT CHAMBERS IN APPLIED INVESTIGATIONS†

V. Perez-Mendez*

Lawrence Berkeley Laboratory
University of California
Berkeley, California 94720

ABSTRACT

In this paper we review various applications of Multiwire Proportional Chambers (MWPC) to problems in Medical Imaging of X-Rays and γ-rays, technical Neutron Radiography, X-Ray Crystallography and X-Ray Astronomy. Various types of drift spaces, gas fillings and solid (Boron, Plastic, Lead) converters for enhancing the detection efficiency of the MWPC to gamma and neutron radiations are discussed.

†Research carried out under the auspices of the U. S. Energy Research and Development Administration.

*Also at Radiology Department, U.C. San Francisco.

Proportional and Drift Chambers in Applied Investigations

V. Perez-Mendez
Lawrence Berkeley Laboratory
Berkeley, California

INTRODUCTION

Multi-wire proportional chambers (MWPC) were developed at CERN (1) starting in 1968 as position sensitive detectors for particle physics research as successors to the Spark Chamber detectors which had been in use for the previous 10 years. Since all of these gas filled devices are capable of detecting low energy γ rays and Thermal neutrons when filled with the appropriate gases, Xenon and ^3He respectively, their potential use in gamma and neutron imaging was soon recognized. Spark Chamber cameras for Nuclear Medicine were developed at Saclay(2) at Michigan (3) and by our group at Berkeley(4). The two main limitations of Spark Chamber γ imaging cameras were the low detection efficiency for γ ray energies normally used in Nuclear Medicine (60~360keV) and the event rate which is limited to less than 10^3 events/sec by the recovery time of the chamber. Since MWPC are capable of event rates which are limited primarily by the capacity of the readout electronics and which can readily be in excess of 10^5 events/sec as well as being inherently simpler in their operation, it is not surprising that they have superseded Spark Chamber in these imaging applications.

Another approach to γ imaging using the ionization mechanism is to use liquid Xenon as the detection medium. Research into liquid Xenon MWPC is underway at Berkeley(5) and at Saclay(6). At this point useful imaging devices using liquid Xenon have not yet been constructed due to the technical difficulties in maintaining the extremely high purity of the Xenon needed for satisfactory operation with reasonable (>10^3) avalanche gain.

The non physics uses of MWPC that we will discuss below in Technical, Medical and Biophysics investigations, involve the imaging applications of γ rays ranging in energy from 8-500keV and Neutrons from thermal energies up to a few MeV(7). Since both of these are uncharged and their detection is accomplished by a secondary charged particle produced either in the gas volume of the detector or from suitable solid converters, good efficiency is obtained only if both the X and Y coordinates of an event are determined from a single avalanche process within a MWPC. With suitable chamber construction these coordinates can be read out electronically by the Delay line method (8), the Pulse Rise time method (9) or by various forms of the Pulse division, Pulse center of gravity methods (10).

The Drift Chamber principle which is now in use in various physics applications (11,12), is not suitable for these technical and Biomedical applications since in general the determination of the X,Y coordinates of the charged particle require timing measurements on two or more avalanches. However, as seen below, the electron drift mechanism is used in many of the medical and biophysical applications to displace

the electrons from one region of the chamber where they are produced to another one where an avalanche is formed and its coordinates read out by any of the methods mentioned previously. The coordinates of the ionizing event - where the γ ray or neutron interacted within the chamber - can be subsequently determined by suitable analogue or digital electronics from the known configuration of electric fields within the chamber. From the various Technical and Biomedical applications in which MWPC have been applied we will discuss the following:

(a) Radiography - X-rays
(b) Radiography - Thermal Neutrons
(c) Nuclear Medicine Imaging - Single γ rays
(d) Nuclear Medicine Imaging - Annihilation γ from Positrons
(e) X-ray Crystallography
(f) X-ray Astronomy

II. Basic Chamber Construction, Digitized Readout and Display

In all of these applications, there will be some differences in the chamber construction depending on whether the ionizing event occurs in the chamber gas or in some solid converter. The readout section of the chamber is fairly similar and is shown schematically in Fig. 1. It consists of three grids of parallel wires: the spacing between grids varies from 3-10 m.m. and that between the anode wires varies from 1-5 m.m. depending on the size of the chamber and the spatial resolution required.

The center grid on which the avalanche multiplication occurs, consists of gold plated tungsten or Stainless Steel wires typically 12-25 microns in diameter. This grid is held at a high positive potential relative to the two outside ones. In order to increase the sensitive region of the chamber for γ or neutron detection, drift regions on one or both sides of the cathode planes are often provided with suitable electric fields. In Fig. 2 we show examples of such drift regions. The simplest (Fig. 2a) is a parallel drift space between the cathode plane and the outer metal walls of the chamber container (13,14). Fig. 2b shows a drift space suitable for use with a pinhole collimator (15) and Fig. 2c shows a spherical - planar drift space for use in X-ray crystallography where the detected radiation originates from a point-like source (16). The X,Y coordinates of an ionizing event can be determined from any two grids of the MWPC. For simplicity, in the chamber configuration shown in Fig. 2a and using a delay line readout, the chamber could be used with all the wires of the central grid connected to a common bus bar from which pulse height information would be obtained. The two outer grids typically consisting of 50-200 micron diameter wires would form an orthogonal X,Y system.

In these grids we make use of the prompt, positive signals induced on them by the avalanche process after the electrons have been collected on the central grid wires. In order to enable the induced signals on the ground plane wires to produce a voltage signal of the right shape for delay line readout these ground grid wires are decoupled from each other and ground through 200 kΩ isolating resistors. The construction and characteristics of the delay lines have been described in detail elsewhere(8).

A signal that indicates the occurrence of an ionizing event is obtained from the central plane through an RC network with a time constant of 500 nsec. This signal is processed by the technique of differentiation and zero-crossing, and is used to start two time-to-height converters. Similarly processed signals obtained from each delay line are used to stop the converters, one from the x-coordinate line and one from the y-coordinate line.

Analog image reconstruction and display is done by using the outputs from the time-to-height converters to drive the x-y deflection plates of a CRT, while simultaneously a z unblank signal is applied, as shown in Fig. 3a. The resultant pattern of dots may then be photographed from the CRT screen. Rates up to 10^5 events/sec have been recorded when a pile-up rejector circuit was used to eliminate multiple events occurring within the delay lines' delay interval and the dead time of the electronics. This rate is presently limited by the recording electronics. The chambers and the delay line themselves have a dead time of less than 1 μsec.

An alternative method of recording the images (shown schematically in Fig. 3b) is to digitize the time-delay signals from the chamber by use of a clock and 200-400 MHz scalers, and then store the coordinates of each event on magnetic tape, disc, or random-access core.

III. Special Chambers for X-ray and Neutron Radiography

(a) X-radiography

For the detection and imaging of x-rays, xenon is used as the principal constituent of the proportional gas. Although the ultimate resolution of these chambers is inferior to that of film, the comparison of picture quality is not too unfavorable, since factors other than film resolution frequently limit the performance of more conventional x-rays systems (i.e., focal-spot, geometry, small-angle scattering, subject movement, etc.). Since the chambers operate in the proportional mode, they also yield the energy of the detected photon with spectral discrimination on the order of 15% FWHM. Thus, they can be used for the imaging of characteristic radiation, or to select a narrow band of x-ray energies from the wide-range output of a standard tube. This permits optimization of energy, and therefore contrast, for the study of interest.

X-ray imaging studies were performed with a 20 x 20 cm^2 chamber, with drift regions on both sides of the wire planes (See Fig. 2a) giving a total xenon mass of 2.2×10^{-2} g/cm^2. This corresponds to a total conversion thickness of 4 cms at 1 atmosphere.

We determined the modulation transfer function (MTF) of the chamber along the x and y directions by recording the data from three resolution-grid patterns consisting of lead slats 4, 2, and 1 mm wide spaced by 4, 2, and 1 mm distances respectively. The object contrast is taken to be 100%, so the value of the MTF is determined from the measured image contrast. For these tests we used a 22 keV Cd-109 source 3mm in diameter placed 12 cm above the grid pattern, which was located on the face of the chamber. The MTF fitted to the data points and corrected for source size is shown in Fig. 4. Fig. 5 shows transmission pictures

obtained with this chamber by using 22 keV sources. The delivered radiation doses for these pictures are quite small. However, they represent 2 to 5 x 10^4 events-cm^2 corresponding, at the present maximum data collection rate of the system (~10^5 sec^{-1}), to exposure times on the order of 1/4 - 1/2 sec-cm^2 of image.

Therefore, the system as now realized would be useful chiefly for specialized applications where either the subject of interest can be immobilized or where resolution is not of paramount importance but dosage is. Prolonged medical fluoroscopy, presently requiring large radiation doses, is an obvious potential application, particularly if the data collection rate was increased beyond the limit presently imposed only by the imaging electronics.

(b) Neutron Radiography

The basic system is modified for neutron imaging by coating the inside surfaces of the chamber windows with material that converts neutrons to charged particles. Thermal and epithermal sensitivity may be achieved with a B-10 coating and fast-neutron sensitivity with a polyethylene coating. Because of the chamber's proportional response, the heavy charged particles produced in these converting materials are easily distinguished from gamma and x-ray background.

We have calcualted that with two optimum-thickness converting surfaces of B-10 for thermal and epithermal neutrons and a single surface of CH_2 for fast neutrons such a chamber can have the efficiency characteristics shown in Table 1.

Table 1. Calculated neutron detection efficiency of wire chamber

Neutron spectrum	Efficiency (%)	Approximate neutron dose at chamber for a 1 n-mm^{-2} image (n - cm^{-2})	(mrem)
Thermal	7	1.4 x 10^3	1.5 x 10^{-3}
1 eV	1.2	8.0 x 10^3	8.0 x 10^{-3}
Fission	0.1	1.0 x 10^5	3.4
14 MeV	0.3	3.2 x 10^4	2.2

The image in Fig. 6 was obtained using Xenon filled (95% Xe; 5% CH_4) chamber at atmospheric pressure. This chamber had two Boron conversion screens which are made by sprinkling finely divided ^{10}B powder mixed with adhesive on the inner surfaces of the flat container windows of the chamber (17). The measured detection efficiency for Thermal neutrons was 5% - somewhat lower than our calculated efficiency (Table I). Higher efficiencies can be obtained using a pressurized He^3 filled chamber (14) or by use of the converter techniques described below.

IV. Nuclear Medicine Imaging

(a) Single Photon Detection

In this application Xenon filled chambers are used to image the spatial distribution of an internally administered gamma emitting radioisotope (18). The optics of the imaging is accomplished by usingaa pinhole collimator placed between the object and the chamber or a parallel hole collimator placed immediately in front of the chamber (Fig. 6). In order to increase the detection efficiency, large drift regions, pressurized chambers or both can be used. The pinhole focused electric field drift arrangement shown in Fig. 2b is especially efficient for this purpose.

In our work we have used a number of chambers with parallel drift regions as shown in Fig. 2a, ranging in size from, 20 x 20 cms to 50 x 50 cms detection area operated at 1-4 atmospheres. Fig.(8) shows the image of a rabbit taken with the 44 keV γ ray emitted by Dysprosium-159, complexed to a radiopharmaceutical which is preferentially absorbed in the bones. For imaging with the 140 keV gamma from Tc-99m - a radioisotope which is used extensively in Nuclear Medicine because of its convenient half life, energy and dosage characteristics - we built a pressurized chamber (4 atmospheres), 6cm parallel plane drift space and with a sensitive area of 20 x 20 cms (19). Figure 9 shows the detection efficiency as a function of gamma ray energy and Figure 10 shows pieture of bar patterns taken with 60 keV and 140 keV gamma rays. Larger chambers (30x30cm) to be used at 10 atmospheres pressure are under construction. Figure 11 shows images of a Picker Thyroid Phantom filled with Tc-99m, and of a rat skeleton and liver/spleen labeled with Tc-99m. Polyphosphate and Sulfur-colloid respectively.

(b) Positron Annihilation Detection

Imaging of gamma rays with energies above 140 keV can be accomplished by use of lead or other high Z converters placed near the cathode wires. The 511 keV annihilation photons from Positron emitters - detected singly or in two coincident detectors are of great interest to Nuclear Medicine since there are many positron emitting isotopes of biological interest including the fact that the only γ emitting isotopes of carbon, oxygen and nitrogen that are usable are positron emitters.

Planar lead converters have low detection efficiency for 511 keV gamma rays (0.26%) since the effective range for the photo and compton electrons is less than 100 microns - and hence the useful detection volume of the lead is confined to a thin surface layer. A feasible way to increase the detection efficiency of such lead converters is to increase the surface area from which conversion electrons can emerge into the sensitive gas region of the MWPC. The technique we have adopted (20) is to use honeycomb shaped lead converters made of lead layers plated on to copper clad mylar(Fig. 12). By applying suitable voltages on to the honeycomb strips, electric fields are produced which drift the conversion electrons into the avalanche region of the MWPC. A section of such a lead converter is shown in Fig. 12b. The detection efficiency of such a lead converter depends on the size of the cell, the height and the probability for drifting out the electrons.

The spatial resolution of the chamber also depends on the cell size. Table 2 below shows our detection efficiency for converters of different sizes (21).

Table 2

Converter cell	surface area / cross sect. area	ϵ_{cal}	$\epsilon_{exp.}$	$\frac{\epsilon_{exp.}}{\text{plane}}$	extraction efficiency
Pb(511 keV gamma)	A_s/A_c	%	%		
Plane converter	1	0.26	0.26	1.0	1.00
3mmx3mm x 12mm	16	4.16	3.20	12.3	0.76
2.2mm x 2.2mm x 12mm	22	5.72	4.20	16.2	0.73
2mm x 2mm x 4mm	8	2.08	1.55	5.4	0.74
Neutron converter Polyethylene (Pu^{238}- Be neutron fission spectrum)					
Plane converter	1	0.11	0.11	1.0	1.00
3.6mm Dia.x 12mm	8	0.18	0.15	1.4	0.83

Alternative approaches to this conversion efficiency were done by the CERN group (22) who drifted the electrons out of a close packed array of lead glass tubes and from a stack of lead and plastic layers with holes of 1-2m.m. size etched into them as shown in Fig. 13, and who obtained a comparable efficiency to our 2.2m.m. honey comb converters.

A positron camera consisting of two detector boxes 48 x 48cm area, 50cm spacing between boxes with MWPC and honeycomb lead converters has been built at LBL and is now in experimental clinical use at the Nuclear Medicine Lab of U.C. San Francisco (23). As shown schematically in Fig. 14 imaging with the two 511 keV annihilation γ rays is accomplished by detecting them in time coincidence with a resolving time of 300 nanosec. This long resolving time is due to the time spread which has to be allowed for in the drifting of electrons originating from different depths within the converter. In order to minimize this time spread we used a gas filling 70% Ar - 30% CH_4 which has a maximum drift velocity for electrons of 10cm/usec. With two honey-comb lead converters in each detector box, cell size 3.5m.m., height 1.2cm we measure an overall spatial resolution of 6m.m. and an overall sensitivity of 700 counts/min/μ curie of positron emitting objects located in the center of the camera. This very high imaging efficiency is one of the main advantages of this camera since no collimators are used. Fig. 14b shows images of Cu-64 wire loops in the mid plane of the camera. Fig. 15 shows an image of a dog labeled with F-18, a positron emitter which is a bone seeking

chemical. The simple reconstruction program that we have used in obtaining this image projects the lines joining the coordinates of each annihilation pair detected by the camera on to a series of planes within the object. Thus structures of the object lying on any given plane will appear to be in focus on it; the contribution of the rest of the object is blurred background. More powerful reconstruction methods which provide 3 dimensional reconstruction by eliminating the blurred background are now being developed for future clinical use.

V. Biophysical Applications

(a) X-ray Crystallography

In organic crystals of large molecular weight, measurement of the intensities of the diffraction spots with conventional techniques encounters difficulty due to the large number of reflections needed and to the low diffracted intensities. Furthemore, many of these crystals are quite fragile and deteriorate rapidly while exposed to the x-ray beam.

Hence a large area detector with the ability to digitize the intensity of the diffracted spots over a large dynamic range provides a useful complement to standard techniques for diffraction intensity measurements.

In collaboration with the University of California, San Diego group (24), we have built a 30 x 30cm sensitive area MWPC with a thin front window for use in x-ray crystallography using the 8 keV K line of copper. The front window is made of Beryllium foil for low attenuation of the incident 8 keV x-rays. The chamber is filled with a Xenon CH_4 mixture at a pressure of 1 atmosphere which is closely regulated to the ambient external pressure by a differential manometer. This chamber has a planar configuration similar to that in Fig. (2a). There is no front drift space; the Beryllium window serves as the front cathode, the anode plane and rear cathode plane are made of wires with diameters of 25 and 100 microns respectively. The Beryllium - Anode space (1cm) is the interaction volume for 8 KeV x-rays and has an efficiency larger than 80%. X,Y coordinate readout is accomplished by two delay lines; one coupled to the anode plane and one to the cathode plane. Zero time, when the avalanche is produced, is determined from the ground plane of one delay line which is connected to ground through a low (<20 ohm) impedance amplifier.

Since in organic crystal structure determinations it is the intensity distribution of the diffraction spots which has to be measured accurately, the response sensitivity of the chamber over all of its surface area is mapped by recording on a computer the response to an 8 keV γ source placed in the position of the crystal. Initial results on the structure of the protein Subtilisin have been reported elsewhere(24).

An alternative approach to x-ray crystallography has been proposed by the CERN group. (16). They have built a chamber with a spherical drift space (See Fig. (2c) backed by a planar chamber from which the X,Y coordinate readout is accomplished.

(b) Chromatography and Electrophoresis with Radioisotopes

Paper Chromatography and Electrophoresis are techniques by which organic compounds can be separated by their different spatial deposition on some suitable planar substrate. When labelled with radioactive isotopes this distribution can be mapped using a MWPC with the configuration shown in Fig. 2a.

For example very efficient electrophoresis separation of proteins labeled with I-125 can be done using the Raymond apparatus (25). Eight 1cm square wells of purified thyroid binding a globulin were molded into the bottom of the well. After electrophoresis, the gel was placed on a chamber with a parallel hole collimator of the type used in Nuclear Medicine imaging. With sample activities as used normally good images of the various components were obtained with 10^4 counts accumulated in periods of 3-5 minutes.

VI. X-ray Astronomy

Very little work has been done so far in x-ray astronomy using MWPC (26), since most of the present generation experiments have used individual proportional counters surveying different directions in space by the rotation of the satellite.

The large area position sensitivity of a MWPC an be honverted into an angular direction determination by use of a pinhole as the photon imaging device. Here again a compromise has to be made between angular accuracy and detection efficiency for photons transmitted through the pinhole.

An elegant method, proposed many years ago for use with x-ray film as the detector is to use a section of a lead Fresnel Zone plate as the imaging device (27). The advantage of using such an imaging aperture in place of the pinhole is that the considerably larger open area of this aperture gives a detection efficiency correspondingly higher than that of the pinhole by the ratio of their respective transmission areas. The resulting distribution of dots can be decoded by appropriate Fresnel - Fourier transformations and the orientation of the point source will be determined. Alternative Coded Apertures using Random Pinhole arrays have been proposed for use in x-ray astronomy (28). We have made a number of mensurements on the imaging capabilities of such coded apertures using Fresnel Zone plates, Random and Non-Redundant pinhole arrays (29); in these applications we used large area (50 x 50cm) Xenon filled MWPC with planar drift regions. At present various groups including one at Chicago, propose to use some of these coded apertures and MWPC detectors in x-ray astronomy (30).

VII. Summary and Conclusions

Multiwire proportional chambers with appropriately shaped drift spaces are excellent detectors for imaging x-ray, gamma ray and neutron distributions. Their main deficiency in this respect has been the low conversion efficiency for producing detectable secondary charged particles. This deficiency can be minimized by the use of high pressure gas fillings together with the various types of drift regions discussed above for

chambers which do not have a very large sensitive area. For higher energy radiations and larger chambers, the use of solid converters with built in drift spaces is more efficient.

The applications discussed here indicate that the use of MWPC in various other scientific and technical fields will prove to be of great value.

Acknowledgements

I would like to thank first my various physics colleagues at LBL with whom I have worked on the development and readout of MWPC: Drs. L. Chang, R. Grove, S. Kaplan, L. Kaufman, C. Lim, B. Macdonald, S. Parker, G. Stoker and K. Valentine. It is a pleasure to acknowledgement the cooperation of the Electronics group at LBL especially K. Lee and F. Kirsten.

The medical applications were done at U.C. San Francisco and the V.A. Hospital, San Francisco in association with Drs. L. Blumin, R. Cavalieri, R. Hattner, M. R. Powell and D. C. Price.

REFERENCES

(1) Multiwire Proportional Chambers, G. Charpak, R. Bouclier, T. Bressani, J. Favier and C. Zupancic. Nuc. Inst. & Methods 62 (1968) 262.

(2) Spark Chambers in Nuclear Medicine, A. J. Lansiart, C. Kellershon. Nucleonic 24 (1966) 56-60.

(3) The Spinthariscope. A new approach to Radiation Imaging, N. H. Horwitz, I. E. Lofstrom and A. L. Forsaith. J. Nuc. Med. 6 (1965) 724-739.

(4) Wire Spark Chambers for Clinical Imaging of Gamma Rays. L. Kaufman, V. Perez-Mendez, A. Rindi, J. Sperinde, H. Wollenberg. Phys. Med. and Biol. 16 (1971) 417.

(5) Liquid Xenon MWPC for Nuclear Medicine Applications. H. Zaklad, S. Dorenzo, T. F. Budinger and L. W. Alvarez. Proc. First World Congress of Nuc. Med. (Tokyo 1974) 362-367.

(6) Detecteurs au Xenon Liquid. A. Lansiart. B.I.S.T. Commissariat a L'Energie Atomique 194 (1974) 25-31.

(7) Multiwire Proportional Chambers for Biomedical Applications, S. N. Kaplan, L. Kaufman, V. Perez-Mendez and K. Valentine. Nuc. Inst. & Methods 106 (1973) 397-406.

(8) Phase Compensated Electromagnetic Delay Lines for MWPC Readout, R. Grove, I. Ko, B. Leskovar, V. Perez-Mendez. Nuc. Inst. & Methods 99 (1972) 381-385; R. Grove, V. Perez-Mendez and J. Sperinde. Nuc. Inst. & Methods 106 (1973) 407-408.

(9) Proportional Counter Photon Camera. C. J. Borkowski and M. K. Kopp. IEEE Trans. Nuc. Sci. NS-17 (1970) 340; NS-19 (1972) 161-168.

(10) High Accuracy Two Dimensional Readout in MWPC. G. Charpak and F. Sauli. Nuc. Inst. & Methods 113 (1973) 381-385.

(11) Some Developments in the Operation of Multiwire Proportional Chambers. G. Charpak, D. Rahm and H. Steiner. Nuc. Inst. & Methods 80 (1970) 13.

(12) The Multiwire Drift Chamber - A New Type of Proportional Wire Chamber. A. H. Walenta, J. Heintze and B. Schurlein. Nuc. Inst. & Methods 92 (1971) 373.
(13) A MWPC for Nuclear Medicine Applications. L. Kaufman, V. Perez-Mendez, D. Shames and G. Stoker. IEEE Trans. Nuc. Sci. NS-19 (1972) 169-172.
(14) A Two Dimensional Position Sensitive Detector for Thermal Neutrons. J. Alberi, J. Fischer, V. Radeka, L. C. Rogers and B. Schoenborn. IEEE Trans. Nuc. Sci. NS-22 (1975) 255-268.
(15) Proportional Counter Radiation Camera. C. J. Borkowski, and M. K. Kopp. U. S. Patent 3,786,270. Jan 1974.
(16) The Spherical Drift Chamber for X-ray Imaging Applications. G. Charpak, Z. Hajduk, A. Jeavons, R. Kahn and R. Stubbs. IEEE Trans. Nuc. Sci. NS-22 (1975) 269-271.
(17) A MWPC for Imaging Thermal, Epicadmium and Fast Neutrons. K. Valentine, S. N. Kaplan, V. Perez-Mendez and L. Kaufman. IEEE Trans. Nuc. Sci. NS-21 (1974) 178-183. The Development of a MWPC Imaging System for Neutron Radiography. K. Valentine. Ph.D Thesis. LBL 2657 (1974).
(18) MWPC in Nuclear Medicine: Present Status and Perspectives. V. Perez-Mendez, L. Kaufman, D. C. Price, M. R. Powell, L. Blumin and R. Cavalieri. LBL 3342 (1974). Proceedings of First World Congress of Nuclear Medicine (Tokyo 1974).
(19) Performance of a Pressurized Xenon Filled MWPC. L. Kaufman, V. Perez-Mendez and G. Stoker. IEEE Trans. Nuc. Sci. NS-20 (1973) 426-428.
(20) Characteristics of MWPC for Positron Imaging. C. B. Lim, D. Chu, L. Kaufmann and V. Perez-Mendez. IEEE Trans. Nuc. Sci. NS-21 (1974) 85-88.
(21) High Efficiency Collimator - Converter for γ and Neutron Imaging with MWPC. D. Chu, C. B. Lim, V. Perez-Mendez, D. Lambert and S. N. Kaplan. LBL 3662 (Jan 1975). To be published - Trans. Amer. Nuc. Soc., New Orleans (June 1975)
(22) High Density Drift Spaces. A. P. Jeavons, G. Charpak, and R. J. Stubbs. IEEE Trans. Nuc. Sci. NS-22 (1975) 297-300; Nuc. Inst. & Methods 124 (1975) 491.
(23) Initial Characterization of a MWPC Positron Camera. C. B. Lim, D. Chu, L. Kaufman, V. Perez-Mendez, R. Hattner and D. C. Price. IEEE Trans. Nuc. Sci. NS-22 (1975) 388-394.
(24) A MWPC as an Area Detector for Protein Crystallography. C. Cork, D. Fehr, R. Hamblin, W. Vernon, N. H. Kuong and V. Perez-Mendez. J. App. Crystallography 7 (1974) 319-323.
(25) S. Raymond. Clinical Chem. 8 455.
(26) Large Area Soft X-ray Imaging System for Cosmic X-ray Studies from Rockets. P. Gorenstein, H. Gursky, F. R. Harnden, A. De Caprio and P. Bjorkholm. IEEE Trans. Nuc. Sci. NS-22 (1975) 616-619.
(27) Fresnel Zone Plate Imaging. N. O. Young. Sky & Telescope 25 (1963) 8.
(28) Scatter-Hole Cameras for X-rays and Gamma Rays. R. H. Dicke.

Astro. Phys. Jour. 153 (1968) L101-L106.
Astr. Phys. Jour. 153 (1968) L101-L106.

(29) Gamma Imaging Using a Fresnel Zone Plate Aperture, MWPC Detector and Computer Reconstruction. B. Macdonald, L. T. Chang, V. Perez-Mendez and L. Shiraishi. IEEE Trans. Nuc. Sci. NS-21 (1974) 678-684.

(30) Solar X-ray Photography with Multiplex Pinhole Camera. R. L. Blake, A. J. Burek, E. Perimore and R. Puetter. Rev. Sci. Inst. 45 (1974) 513-516.

FIGURE CAPTIONS

Fig. 1 Schematic diagram of Xenon-filled chamber (a) side view, (b) top view showing wire planes and delay lines.

Fig. 2 Side view of MWPC showing various forms of drift regions
(a) Planar drift regions between cathode planes and container walls.
(b) Chamber with large drift space between one cathode and pinhole collimator. A suitable electric gradient is provided by the guard rings.
(c) Chamber with spherical conversion space coupled to a planar wire grids for low energy x-ray detection.

Fig. 3 Electronics block diagrams for (a) analog system with scope display and (b) digital system with storage capabilities.

Fig. 4 MTF for 22 KeV x-rays. The data points show the measured contrast ratios for the centerpoints of the test patterns. The dashed curve is the calculated fit to these points, and the solid curve is the corresponding modulation transfer function. (The sign of the 0.5 mm^{-1} datum point is inferred from the fit.)

Fig. 5 X-ray transmission pictures taken with exposures of (a) 0.015 mR, (b) 0.03 mR, (c) 0.045 mR, and (d) 0.038 mR at 22 keV.

Fig. 6 Neutron sensitive wire chamber image of an aluminum-cased electric drill. The background pattern is produced by a Gadolinium anti-scatter grid of 2 mm aperture. The opaque area between the chuck and the motor is due to the grease in the gear box. The image corresponds to 20 detected netrons/mm^2.

Fig. 7 Relation of chamber, object and collimator for imaging with internally administered radioisotopes (a) Parallel Hole Collimator (b) Pinhole Collimator.

Fig. 8 Image of rabbit labelled with Dy-159 HEDTA and Dy-159 polyphosphate. The vertebrae of the rabbit are seen clearly.

Fig. 9 Detection efficiency of 4 atmosphere Xenon-filled chamber versus gamma energy. Thickness of chamber including drift regions is 6.4cms.

Fig. 10 Transmission bar patterns taken with 4 atmosphere chamber:
(a) 10 mm, (b) 4 mm, (c) 2 mm, (d) 1mm -- taken at 60 keV.
(e) 10 mm, (f) 4 mm, (g) 2 mm,— taken at 140 keV.

Fig. 11 Top image is of Picker Thyroid Phantom filled with Tc-99 solution (300) k counts). Lower images of rat skeleton and liver/spleen Labeled with Tc-99 polyphosphate (300 k counts) and Tc-99m Sulfur Colloid (100 k counts).

Fig. 12 Honeycomb lead converters for 511 keV γ imaging:
(a) Side view of chambers showing relative positions of the converters to the MWPC wire planes.
(b) Photograph of a section of lead converter.
(c) Schematic diagram of honeycomb converter showing drift fields. Detection efficiency depends on fraction of electric lines that drift electrons to the wire planes.

Fig. 13 Alternative type of converters proposed by CERN group.
(a) Stack of lead glass tubes.
(b) Top view of lead-plastic stack with etched holes

Fig. 14 (a) Schematic drawing of positron camera showing object placed between MWPC detector boxes.
(b) Photographs of Cu-64 wire sources in mid-plane of camera showing the detail obtainable with present resolution. The loop is 1.2cm diameter and the parallel wires 1cm apart.

Fig. 15 Image of dog labeled with F-18, a bone seeking positron emitter. The images were reconstructed at different planes within the dog: Thus any portion of the skeleton lying on a given plane is shown in focus for that plane.

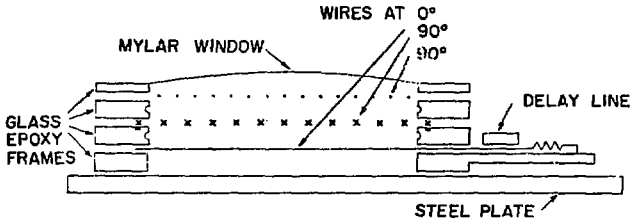
WIRES AT 0°
90°
90°
MYLAR WINDOW
DELAY LINE
GLASS
EPOXY
FRAMES
STEEL PLATE

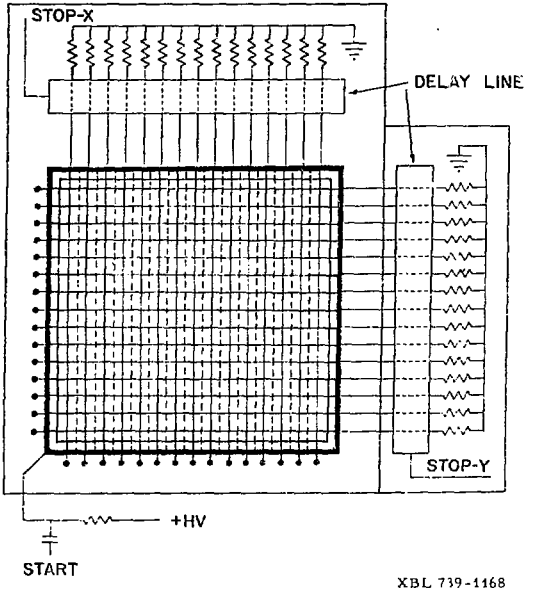
STOP-X
DELAY LINE
STOP-Y
+HV
START
XBL 739-1168

Fig. 1

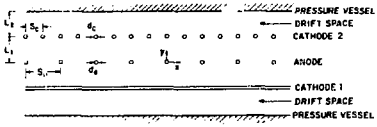

(a)

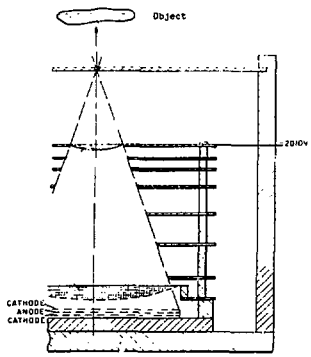

(b)

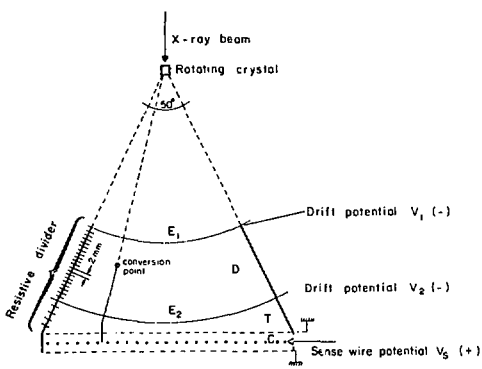

(c)

FIG. 2

XBL 754-1210

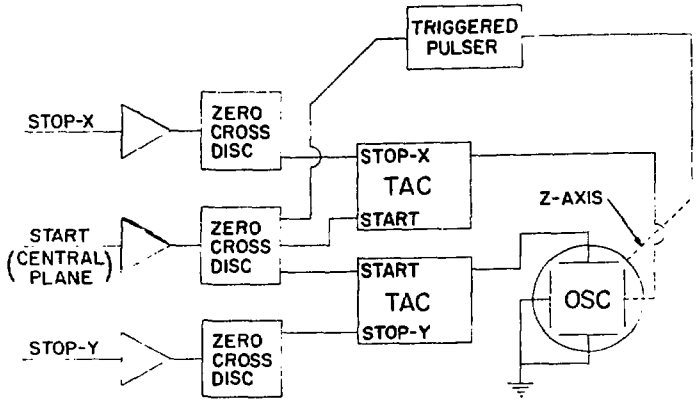
TRIGGERED PULSER
STOP-X
ZERO CROSS DISC
STOP-X TAC
START
Z-AXIS
START (CENTRAL) PLANE
ZERO CROSS DISC
START TAC
STOP-Y
OSC
STOP-Y
ZERO CROSS DISC

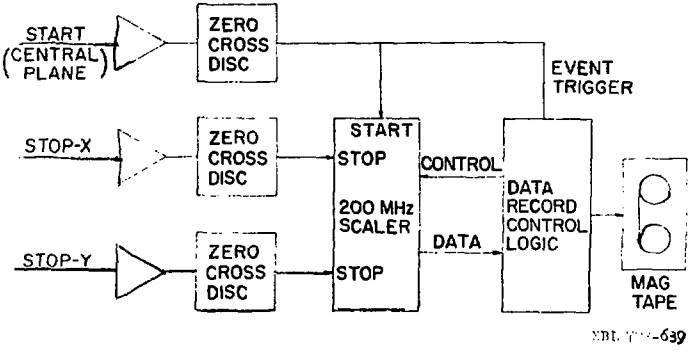
START (CENTRAL) PLANE
ZERO CROSS DISC
EVENT TRIGGER
STOP-X
ZERO CROSS DISC
START
STOP
CONTROL
200 MHz SCALER
DATA
DATA RECORD CONTROL LOGIC
MAG TAPE
STOP-Y
ZERO CROSS DISC
STOP

XBL [illegible]-639

Fig. 3

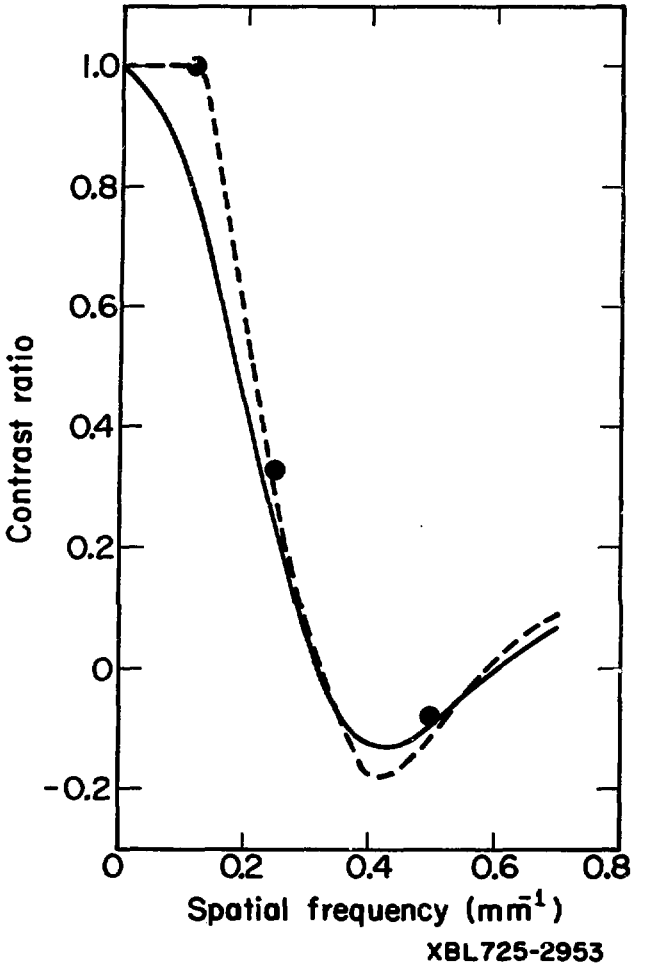
1.0
0.8
0.6
0.4
0.2
0
-0.2
Contrast ratio
0
0.2
0.4
0.6
0.8
Spatial frequency (mm⁻¹)
XBL725-2953

Fig. 4

Fig. 5

XBB 713- 884

XBB 7212-3847

Fig. 6

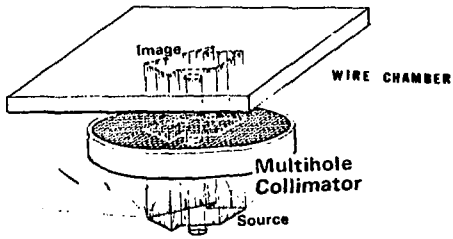

a.

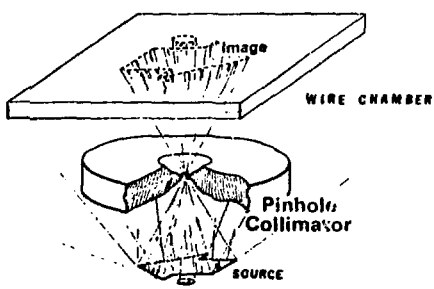

b.

XBL 755-1236

Fig. 7

MULTI-WIRE PROPORTIONAL CHAMBER

RABBIT

^{159}DY-HEDTA

24 HOURS POST

10 MIN

^{159}DY-POLYPHOSPHATE

120 HOURS POST

10 MIN

Fig. 8

XBB 729-4509

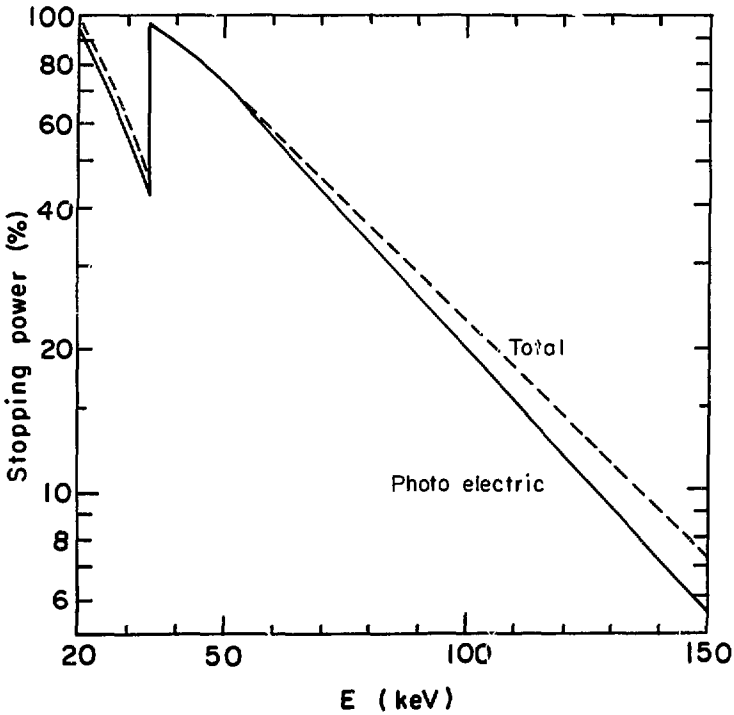
100
80
60
40
20
10
8
6
Stopping power (%)
Total
Photo electric
20
50
100
150
E (keV)
XBL7210-4180

Fig. 9

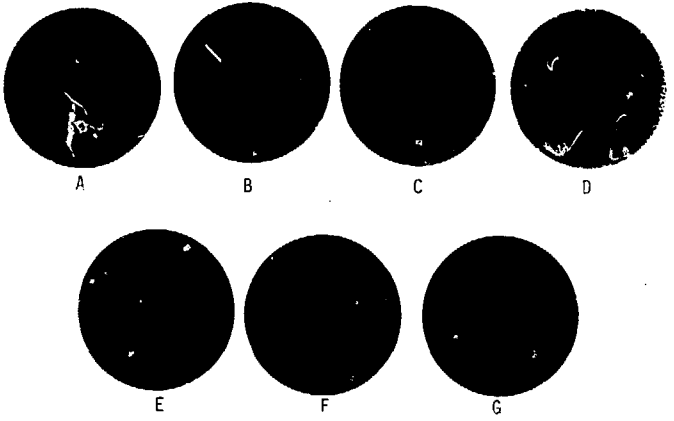

XBB 7210-5305

Fig. 10

THYROID PHANTOM ^{99m}Tc 100 K

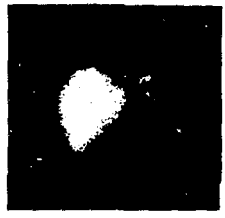

RAT LIVER/SPLEEN ^{99m}Tc Sulfur Colloid
100 K

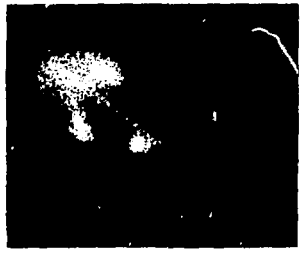

RAT ^{99m}Tc POLYPHOSPHATE 300 K

XBB 748-5949

Fig. 11

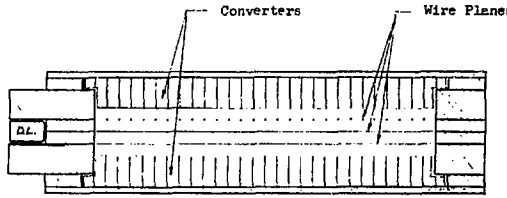

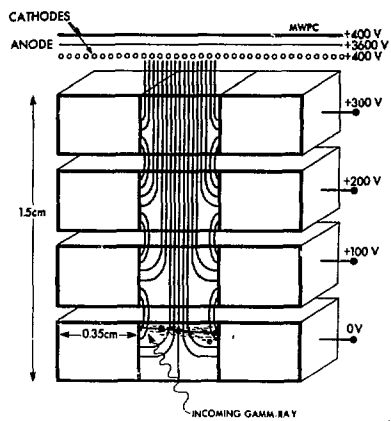

XBB 751-782

Fig. 12

a)

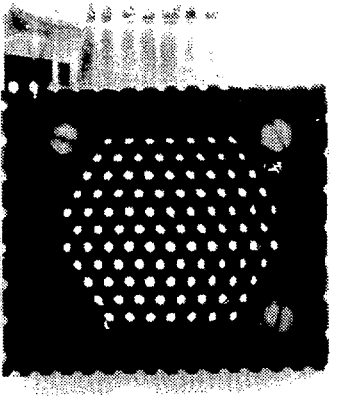

XBB 755-3760

b)

Fig. 13

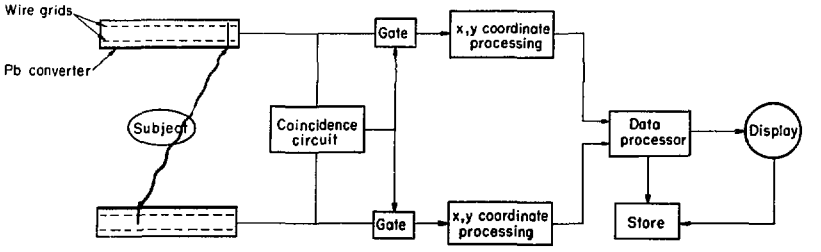

a.

10 cm Full Scale

50 cm Full Scale

b.

XBB 755-3784

Fig. 14

zf = 0 cm

zf = 2 cm

zf = 4 cm

zf = 6 cm

zf = 8 cm

zf = 10 cm

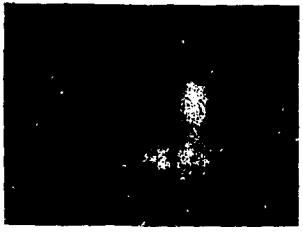

zf = 16 cm

XBB 748-5311